IEEE Access
Multidisciplinary ⋮ Rapid Review ⋮ Open Access Journal

Received 13 April 2024, accepted 13 June 2024, date of publication 24 June 2024, date of current version 15 August 2024.

Digital Object Identifier 10.1109/ACCESS.2024.3418031

RESEARCH ARTICLE

Optimal Structure to Maximize Torque per Volume for the Consequent-Pole PMSM and Investigating the Temperature Effect

ALIREZA HOSSEINPOUR[1], AHMED ABBAS[2], MAHMOUD OUKATI SADEGH[3], ATIF IQBAL[4], (Fellow, IEEE), AYMEN FLAH[5,6,7,8,9], LUKAS PROKOP[10], ENAS ALI[11], AND RAMY N. R. GHALY[12,13], (Student Member, IEEE)

[1]Department of Electrical Engineering, University of Zabol, Zabol, Iran
[2]Faculty of Electrical and Control Engineering, Gdansk University of Technology, 80-233 Gdansk, Poland
[3]Department of Electrical Engineering, University of Sistan and Baluchestan, Zahedan, Iran
[4]Department of Electrical Engineering, Qatar University, Doha, Qatar
[5]National Engineering School of Gabes, University of Gabes, Gabès 6029, Tunisia
[6]MEU Research Unit, Middle East University, Amman 11831, Jordan
[7]Applied Science Research Center, Applied Science Private University, Amman 11931, Jordan
[8]College of Engineering, University of Business and Technology (UBT), Jeddah 21448, Saudi Arabia
[9]Private Higher School of Applied Sciences and Technology of Gabes, University of Gabes, Gabès 6029, Tunisia
[10]ENET Centre, VSB—Technical University of Ostrava, 708 00 Ostrava, Czech Republic
[11]University Centre for Research and Development, Chandigarh University, Mohali, Punjab 140413, India
[12]Ministry of Higher Education, Mataria Technical College, Cairo 11718, Egypt
[13]Chitkara Centre for Research and Development, Chitkara University, Punjab, Himachal Pradesh 174103, India

Corresponding authors: Alireza Hosseinpour (a.hoseinpour@uoz.ac.ir) and Aymen Flah (aymen.flah@enig.u-gabes.tn)

This work was supported in part by the University of Zabol Collaborative Research under Grant IR-UOZ-GR-1799, in part by European Union under the REFRESH—Research Excellence for Region Sustainability and High-Tech Industries under Project CZ.10.03.01/00/22_003/0000048 via the Operational Programme Just Transition, in part by the National Centre for Energy II and ExPEDite Project a Research and Innovation Action to Support the Implementation of the Climate Neutral and Smart Cities Mission Project under Grant TN02000025, and in part by European Union's Horizon Mission Program through the Project ExPEDite under Agreement 101139527.

ABSTRACT Heat removal, maximizing torque, minimizing losses, volume, cost, and temperature effect play essential roles in electrical vehicle applications. An inner-rotor consequent-pole permanent magnet synchronous machine (CPPMSM) merits suitable losses, cost, and heat rejection. Hence, first, a two-dimensional model of CPPMSM is explained based on solving Maxwell's equations in all regions of the machine. Then, all the components of torque, back-EMF, inductance, and unbalanced magnetic forces in the direction of the X-axis and Y-axis and their magnitudes are calculated. Afterward, the overload capability and the torque-speed characteristic are determined based on the average torque. Therefore, to maximize the torque/volume ratio, four metaheuristic optimization algorithms, including Genetic Algorithm (GA), Particle Swarm Optimization (PSO), Differential Evolution (DE), and Teaching Learn Base Optimization (TLBO), have been implemented, and the mentioned index is optimized. Since the said algorithms usually can minimize, its inverse is minimized instead of the index mentioned above being maximized. At this stage, the effect of three types of magnetization patterns, i.e., radial, parallel, and bar magnet in shifting, is also considered. The flux density of the permanent magnet changes concerning temperature. Finally, the effect of these changes on cogging, reluctance, and instantaneous torque, as well as back-EMF, unbalance magnetic force (UMF), torque-speed characteristic, and overload capability diagram, will be analyzed. The simulation was performed using MATLAB software.

The associate editor coordinating the review of this manuscript and approving it for publication was Xiaosong Hu.

INDEX TERMS Electric vehicle, magnetization pattern, meta-heuristic optimization algorithms, temperature impact.

I. INTRODUCTION

Electric vehicles need suitable heat removal, maximum torque, minimum losses, cost, and volume. The CPPMSMs have special features compared to superficial permanent magnet machines. These machines use fewer magnets [1], [2], making them more economical and reducing eddy current losses [3]. Also, due to the presence of iron between the magnets, the passage of the armature reaction (AR) field through iron increases, which helps reduce the eddy current losses in the magnet even more [3]. In addition, the flux linkage increases in this type of machine [4], and the structure used in the present paper increases the torque by raising the reluctance torque [5]. Thus, it is an appropriate option for the mentioned application. The design of this type of electric machine requires an accurate model due to the asymmetric distribution of flux in the air gap under adjacent poles.

Although numerical methods [6] provide an accurate answer, the main disadvantage of these methods is the lack of a function for indicators such as torque and back-EMF. Therefore, such methods are not used for optimization. The equivalent circuit method examines only magnetic flux density changes in the radial direction and ignores changes in the tangential direction [7]. Also, in these methods, in exchange for changes, the number of poles, slots, etc., the equivalent circuit must be redrawn, and the desired indicators must be calculate; hence, using them for optimization is not recommended. Furthermore, only the radial magnetization pattern can be modeled in the equivalent circuit method, and the effect of other magnetization patterns remains unknown. To solve the mentioned problems, a two-dimensional analysis based on solving Maxwell's equations in sub-regions has been proposed [7].

CPPMSMs are of two types, i.e., outer-rotor [8] and inner-rotor consequent-pole machines [3]. The first one has more torque due to the larger radius of the rotor; however, not only their heat removal but also their starting and braking are more difficult. On the other hand, in the CPPMSM inner rotor (CPPMSMIR), heat rejection is performed better, and the machine has less inertia. The machine used in electric vehicles must have the lowest cost, adequate heat removal, acceptable acceleration and declaration, and the highest torque/volume ratio. To reduce costs and losses, a consequent-pole machine is used; to reject heat better, the CPPMSMIR is preferred; and to compensate for the torque loss, the machine needs to be designed to maximize its torque. Therefore, the torque must be determined as a function of machine parameters; then, this function needs to be maximized by derivative-based methods or metaheuristic methods. Previously, a model was proposed for a permanent magnet machine with double excitation on the rotor based on the finite element method (FEM) method. Then, the target indicators for optimization were determined using the curve fitting method as a function of the pole arc-to-pole pitch ratio [9]. In addition, the performance of the said machine was approximated by considering the larger number of inputs to the neural network [10]. Further, the hybrid machine has been analyzed in two dimensions, and the number of poles and the armature winding type have been modified to reduce torque ripple. In addition to the above, the number of rotor slots has also been changed to reduce UMF. The effect of the changes in the number of poles and slots for the inner-rotor [3] and outer-rotor consequent-pole machine [8] has been investigated. Also, the torque can be increased by deforming the poles [11] and modifying the rotor structure [12]. The effect of temperature and magnetization patterns has been investigated. In addition to the mentioned methods, there is another one which is a magnetic equivalent circuit [13]. It computes the back-EMF, torque and inductances. In contrast, the reluctances are time-variant and position dependent. Also, it can't model magnetization patterns. As a result, it doesn't accurately calculate all machine indicators [7].

In this paper, using the two-dimensional method, the flux density is calculated, and then, based on it, the torque is also calculated. Due to the large number of variables, the use of metaheuristic optimization algorithms is recommended, which has been done using the four methods GA, PSO, DE, and TLBO [14], [15], [16], [17] in the current study. These algorithms are population-based, that is, first a primary population is generated. Then, by considering some points related to each method, the population is improved in the next generations. Until the stopping condition happens. Furthermore, because the permanent magnet's magnetic field (PM) significantly affects the torque, three types of magnetic patterning, i.e., radial, parallel and bar magnet in shifting, have been considered. After obtaining the optimal characteristics, the torque-speed characteristic, the overload capability, the self and mutual inductance of the stator winding, Back-EMF, and UMFs in the X and Y axes as well as the magnitude of these magnetic pulls are obtained. Finally, the effect of temperature on the mentioned indicators in the optimized machine is investigated. Structure of CPPMSM is presented in Fig. 1.

II. TWO-DIMENSIONAL ANALYSIS OF CPPMSM

A. RADIAL AND TANGENTIAL FLUX DENSITY

To derive a two-dimensional model, Maxwell's equations must first be solved in all regions of the machine. For this purpose, a series of simplifying assumptions are required for CPPMSMIR zoning, as stated in references [18] and [19].

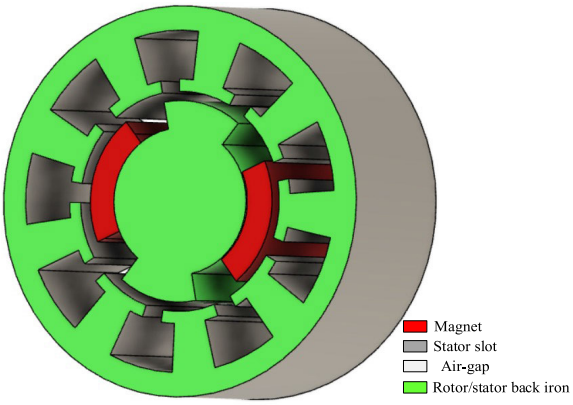

FIGURE 1. 3-D structure of CPPMSMIR.

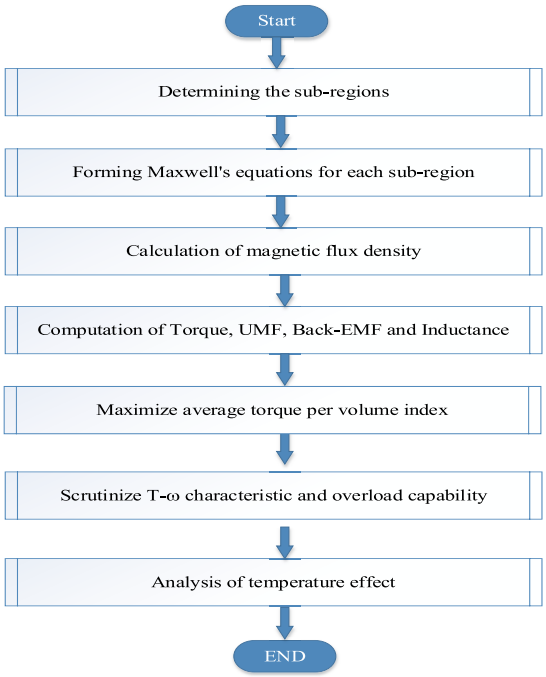

FIGURE 2. The steps of CPPMSMIR analysis.

The steps of doing this study have been shown in Fig. 2. Maxwell's equations are simplified as follows:

$$\frac{1}{r}\frac{\partial}{\partial r}\left(r\frac{\partial A_z^{sls}}{\partial r}\right)+\frac{1}{r^2}\frac{\partial^2 A_z^{sls}}{\partial \theta^2}=-\mu_0 J_z^s \tag{1}$$

$$\frac{1}{r}\frac{\partial}{\partial r}\left(r\frac{\partial A_z^{m}}{\partial r}\right)+\frac{1}{r^2}\frac{\partial^2 A_z^{m}}{\partial \theta^2}=-\frac{\mu_0}{r}(M_\theta-\frac{\partial M_r}{\partial \theta}) \tag{2}$$

$$\frac{1}{r}\frac{\partial}{\partial r}\left(r\frac{\partial A_z^{i}}{\partial r}\right)+\frac{1}{r^2}\frac{\partial^2 A_z^{i}}{\partial \theta^2}=0\ i=\{a,so\} \tag{3}$$

where, a, m, so, s *and* sls are air gap, PM, slot-opening, stator, and stator slot, respectively.

If the Fourier series of stator current density distribution, the radial and tangential components of magnetization patterns, and the boundary and interregional conditions for the above equations are adequately considered [18].

The magnetic flux density is computed using $B=\nabla\times A$, Where for the 2-D analysis, they are obtained using Equations (4) and (5).

$$B_r(r,\theta)=\frac{1}{r}\frac{\partial A_z}{\partial \theta} \tag{4}$$

$$B_\theta(r,\theta)=-\frac{\partial A_z}{\partial r} \tag{5}$$

B. INSTANTANEOUS, COGGING, AND RELUCTANCE TORQUE

The instantaneous torque (T_{inst}) of a CPPMSM is calculated based on Maxwell stress tensor according to Equation (6).

$$T_{inst}=\frac{L}{u_0}\int_{-\pi}^{\pi}\left(B_{r,PM}^a+B_{r,AR}^a\right)\left(B_{\theta,PM}^a+B_{\theta,AR}^a\right)\Big|_{r=R_c}R_c^2 d\theta \tag{6}$$

where $B_{r,PM}^a, B_{r,AR}^a, B_{\theta,PM}^a,$ and $B_{\theta,AR}^a$ are the radial and tangential magnetic flux density components due to PMs and AR in the air gap, respectively.

Equation (6) calculates the total torque. Cogging (T_{cog}), Reluctance (T_{re}), and mutual (T_{mu}) torque waveforms can be obtained separately from equations (7) to (9).

$$T_{cog}=\frac{L}{u_0}\int_{-\pi}^{\pi}\left(B_{r,PM}^a\right)\left(B_{\theta,PM}^a\right)\Big|_{r=R_c}R_c^2 d\theta \tag{7}$$

$$T_{re}=\frac{L}{u_0}\int_{-\pi}^{\pi}\left(B_{r,AR}^a\right)\left(B_{\theta,AR}^a\right)\Big|_{r=R_c}R_c^2 d\theta \tag{8}$$

$$T_{mu}=\frac{L}{u_0}\int_{-\pi}^{\pi}\left(B_{r,AR}^a\right)\left(B_{\theta,PM}^a\right)+\left(B_{\theta,AR}^a\right)\left(B_{r,PM}^a\right)\Big|_{r=R_c}R_c^2 d \tag{9}$$

All torque components are calculated due to only the air gap magnetic flux density.

C. UNBALANCE MAGNETIC FORCE

The Maxwell stress tensor computes the radial and tangential forces exerted on the stator surface. These magnetic pulls are calculated based on the magnetic fields in the air gap.

$$f_r=\frac{1}{2\mu_0}\left(B_r^2-B_\theta^2\right) \tag{10}$$

$$f_\theta=\frac{1}{\mu_0}B_rB_\theta \tag{11}$$

These equations can be transformed into the Cartesian system.

$$f_x=f_r\cos(\theta)-f_\theta\sin(\theta) \tag{12}$$

$$f_y=f_r\sin(\theta)+f_\theta\cos(\theta) \tag{13}$$

Then, UMF is determined by integrating these forces in the middle of the air gap.

$$F_x(t)=\int_{-L/2}^{L/2}\int_{-\pi}^{\pi}f_x r d\theta dz=L\int_{-\pi}^{\pi}f_x r d\theta \tag{14}$$

$$F_y(t)=\int_{-L/2}^{L/2}\int_{-\pi}^{\pi}f_y r d\theta dz=L\int_{-\pi}^{\pi}f_y r d\theta \tag{15}$$

$$F_r = \sqrt{F_x^2 + F_y^2} \tag{16}$$

The magnitude of the unbalanced magnetic forces and their components are computed only by the air gap magnetic flux density.

D. BACK - EMF

The path of the flux passing through a stator tooth is shown in Fig. 3. It can be computed with Gauss's law.

$$\begin{aligned}\oint B.ds = 0 \rightarrow \varphi_{16} &= \varphi_{12} + \varphi_{23} + \varphi_{34} + \varphi_{45} + \varphi_{56} \\ &= \int_{s_{12}} B.ds + \int_{s_{23}} B.ds + \int_{s_{34}} B.ds \\ &\quad + \int_{s_{45}} B.ds + \int_{s_{56}} B.ds \end{aligned} \tag{17}$$

Using constant coefficients in the machine's analytical model, the flux of one turn of the jth winding, which is wrapped on the jth tooth in the non-overlapping winding, is obtained from the following equation.

$$\begin{aligned}\varphi_j(\alpha) = L \sum_{v_s=1}^{V_s} &\left[\left(\frac{R_{so}}{R_{sl}}\right)^{\frac{2\pi v_s}{\delta_s}} + 1\right] \\ &\times \left\{ b_{v_s}^{sls,j} \left[\cos\left(\frac{\pi v_s}{\delta_s}\left(\frac{\delta_s + \beta}{2}\right)\right)\right.\right. \\ &\left. -(-1)^{v_s}\right] - b_{v_s}^{sls,j+1}\left.\left[\cos\left(\frac{\pi v_s}{\delta_s}\left(\frac{\delta_s - \beta}{2}\right)\right) - 1\right]\right\} \\ &+ \mathrm{L}\sum_{u=1}^{U}\left[(a_u^{so,j+1} - (-1)^u a_u^{so,j})\right. \\ &\left. - (b_u^{so,j+1} - (-1)^u b_u^{so,j})\right]\left[\left(\frac{R_s}{R_{so}}\right)^{\frac{\pi u}{\beta}} - 1\right] \\ &- 2L\sum_{n=1}^{N}\left\{\left[a_n^a + b_n^a\left(\frac{R_m}{R_s}\right)^n\right]\sin\left(n\delta_{j+1}\right)\right. \\ &\left. - \left[c_n^a + d_n^a\left(\frac{R_m}{R_s}\right)^n\right]\cos(n\delta_{j+1})\right\}\sin(\frac{n\theta_t}{2}) \end{aligned} \tag{18}$$

In the case of all-teeth wound we have j=1,2,…,Qj. In contrast, j=1,3,5,…,Qj-1 for the case of alternate-teeth wound. Moreover, θt=2π/Qj-β is the span angle of each tooth and δj = 2π(j − 1)/Qj is the angle of jth stator slot center. In addition, the flux of one turn of jth winding, which is wrapped on the j and j+s teeth in the non-overlapping winding, is obtained from the following equation.

The induced voltage in the jth windings can be achieved using Faraday's law of induction.

$$E_j = -N_t \frac{d\varphi_j}{d\alpha} \tag{19}$$

In this method, the magnetic flux density in the air gap, the stator slot-opening, and the slot are utilized to calculate the induced voltage.

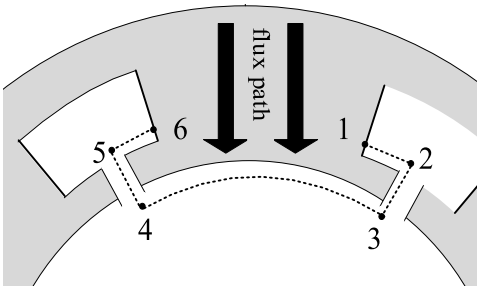

FIGURE 3. Flux path in teeth.

E. INDUCTANCE

To compute the self-and mutual inductances of the stator phases, the flux density caused by the armature current should solely be considered. The flux linkage of jth winding caused by the j′ phase flowing in the non-overlapping windings is calculated from the following equation.

$$\begin{aligned}&\lambda_{j,j'}(\alpha) \\ &= LN_t \sum_{v_s=1}^{V_s}\left[\left(\frac{R_{so}}{R_{sl}}\right)^{\frac{2\pi v_s}{\delta_s}} + 1\right] \\ &\quad \times \left\{ b_{v_s}^{sls,j,j'}\left[\cos\left(\frac{\pi v_s}{\delta_s}\left(\frac{\delta_s + \beta}{2}\right)\right)\right.\right. \\ &\quad \left. -(-1)^{v_s}\right] - b_{v_s}^{sls,j+1,j'}\left.\left[\cos\left(\frac{\pi v_s}{\delta_s}\left(\frac{\delta_s - \beta}{2}\right)\right) - 1\right]\right\} \\ &\quad + \left((b_0^{so,j+1,j'} - (b_0^{so,j,j'}\right)\ln\left(\frac{R_s}{R_{so}}\right) \\ &\quad + LN_t \sum_{v_s}^{V_s}\frac{\mu_0}{\left(\frac{\pi v_s}{\delta_s}\right)^2 - 4}\left[R_{so}^2 + \frac{2R_{sl}^2}{\frac{\pi v_s}{\delta_s}}\left(\frac{R_{so}}{R_{sl}}\right)^{\frac{\pi v_s}{\delta_s}}\right] \\ &\quad \times \left\{ J_{v_s}^{j,j'}\left[\cos\left(\frac{\pi v_s}{\delta_s}\left(\frac{\delta_s + \beta}{2}\right)\right)\right] - (-1)^{v_s}\right] \\ &\quad - J_{v_s}^{j+1,j'}\left.\left[\cos\left(\frac{\pi v_s}{\delta_s}\left(\frac{\delta_s - \beta}{2}\right)\right) - 1\right]\right\} \\ &\quad + LN_t \sum_{u=1}^{U}\left[(a_u^{so,j+1,j'} - (-1)^u a_u^{so,j,j'})\right. \\ &\quad \left. - (b_u^{so,j+1,j'} - (-1)^u b_u^{so,j,j'})\right]\left[\left(\frac{R_s}{R_{so}}\right)^{\frac{\pi u}{\beta}} - 1\right] \\ &\quad - 2LN_t \sum_{n=1}^{N}\left\{\left[a_n^{a,j'} + b_n^{a,j'}\left(\frac{R_m}{R_s}\right)^n\right]\sin\left(n\delta_{j+1}\right)\right. \\ &\quad \left. - \left[c_n^{a,j'} + d_n^{a,j'}\left(\frac{R_m}{R_s}\right)^n\right]\cos(n\delta_{j+1})\right\}\sin(\frac{n\theta_t}{2}) \end{aligned} \tag{20}$$

For j=1,2,…,Qj and j′=1,2,…,Qj; and $J_{v_s}^{j,j'}$ is the vs component of the current density in slot j when all phase currents are zero except for j′.

In addition, the flux linkage of jth windings (between jth and (j+s)th teeth) caused by the j′ phase flowing in the non-overlapping windings is computed using the following equation.

$$\lambda_{j,j'}(\alpha) = LN_t \sum_{v_s=1}^{V_s}\left[\left(\frac{R_{so}}{R_{sl}}\right)^{\frac{2\pi v_s}{\delta_s}} + 1\right]$$

TABLE 1. Fixed parameters of CPPMSMIR that are not optimization parameters.

Parameter	Description	Value
P	Number of poles	4
Q	Number of slots	15
R	Radius of stator	50
I_m	Phase current	10
N	Number of harmonics in air gap	100
W	Number of harmonics in PM	100
V	Number of harmonics in slot-opening	100
U	Number of harmonics in slot	100
f	Frequency	50

$$\times \left\{ b_{v_s}^{sls,j,j'} \left[\cos\left(\frac{\pi v_s}{\delta_s} \left(\frac{\delta_s + \beta}{2} \right) \right) - (-1)^{v_s} \right] - b_{v_s}^{sls,j+1,j'} \left[\cos\left(\frac{\pi v_s}{\delta_s} \left(\frac{\delta_s - \beta}{2} \right) \right) - 1 \right] \right\} + \left((b_0^{so,j+1,j'} - (b_0^{so,j,j'}) \ln\left(\frac{R_s}{R_{so}} \right) \right. + \mathrm{L}N_t \sum_{u=1}^{U} [(a_u^{so,j+1,j'} - (-1)^u a_u^{so,j,j'}) - (b_u^{so,j+1,j'} - (-1)^u b_u^{so,j,j'})] \left[\left(\frac{R_s}{R_{so}} \right)^{\frac{\pi u}{\beta}} - 1 \right] - 2LN_t \sum_{n=1}^{N} \left\{ \left[a_n^{a,j'} + b_n^{a,j'} \left(\frac{R_m}{R_s} \right)^n \right] \sin\left(n\delta_{j+1} \right) - \left[c_n^{a,j'} + d_n^{a,j'} \left(\frac{R_m}{R_s} \right)^n \right] \cos(n\delta_{j+1}) \right\} \sin(\frac{n\theta_t}{2}) \tag{21}$$

In the case of all-teeth wound, we have j=1,2,…,Qj. In contrast, j=1,3,5,…,Qj-1 for the case of alternate-teeth wound.

If there are several series windings in j^{th} windings phase, their fluxes should be added together. Finally, the k^{th} phase inductance due to the k' phase current is calculated with the following equation.

$$L_{k,k'} = \sum_{j \epsilon k, j' \epsilon k'} \frac{\lambda_{j,j'}}{i_{j'}} \tag{22}$$

To achieve the self-inductance, it is required to excite phase k instead of k′. Next, the flux linkage caused by this current is computed. Finally, the self-inductance is determined by the following equation.

$$L_{k,k} = \sum_{j \epsilon k, j' \epsilon k} \frac{\lambda_{j,j'}}{i_{j'}} \tag{23}$$

F. OPTIMIZATION INDEX

The objective function at this stage is to maximize the torque/volume index. It is assumed that the volume is determined according to thermal considerations, and it is constant; therefore, the average torque needs to be maximized because the number of variables affecting the torque is high and the search space is very large. Metaheuristic algorithms are used to determine the optimal dimensions of the machine. Since such algorithms are used for minimization, the inverse is minimized instead of the average amount of torque being maximized. Accordingly, we are faced with an optimization problem.

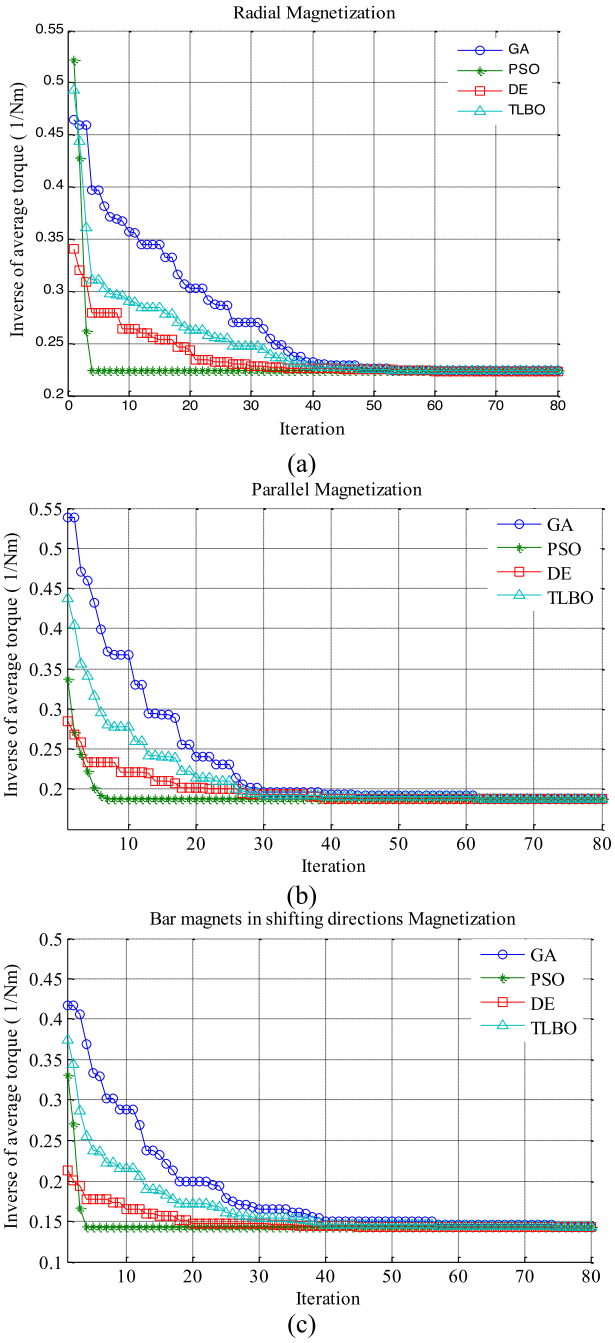

FIGURE 4. The inverse of the average torque for different magnetization patterns a) Radial b) Parallel c) Halbach.

$$Min\ (\frac{1}{T_{ave}(R_r, R_m, R_s, R_{sl}, L, \delta_s, \delta_r, \beta, \alpha_0)}) \tag{24}$$

$$15 < R_r < 20 \tag{25}$$

$$4 + R_r < R_m < 8 + R_r \tag{26}$$

TABLE 2. Optimized CPPMSMIR specifications.

Parameter	Description	Amount
R_{sl}	Outer radius of the slot	45
R_{so}	Outer radius of the slot-opening	32
R_s	Stator bore radius	29
R_m	Magnet radius	28
R_r	Rotor radius	2
L	Axial length of the motor	58
δ	Slot span angle	0.377
β	Slot-opening span angle	0.1131

$$1 + R_m < R_s < 2 + R_m \tag{27}$$
$$1 + R_s < R_{so} < 3 + R_s \tag{28}$$
$$9 + R_{so} < R_{sl} < 13 + R_{so} \tag{29}$$
$$0.3 < \frac{L}{R_s} < 2 \tag{30}$$
$$0.3 * \frac{2\pi}{Q_s} < \delta_s < 0.9 * \frac{2\pi}{Q_s} \tag{31}$$
$$0.3 * \delta_s < \beta < 0.7 * \delta_s \tag{32}$$

Metaheuristic algorithms may get stuck in the local minimum and not converge to the global minimum. Also, their final result depends on the initial guess. To overcome the above problems, the four algorithms GA, PSO, DE and TLBO are considered, and each is executed several times. Finally, their answers are compared.

G. TEMPERATURE EFFECT

If the temperature changes in the range of 0 to 150 degrees, the residual flux density of the permanent magnet decreases with increasing temperature according to Equation (33) [20].

$$B_r = B_{r20}\left[1 + \frac{\alpha_B}{100}(\theta_{PM} - 20)\right] \tag{33}$$

where α_B is 0.105.

The change in residual flux density affects the magnetic field caused by the magnet, and although the changes in this field have no effect on inductance and reluctance torque, they affect instantaneous torque, cogging torque, Back-EMF, UMF, overload capability, and torque-speed characteristic. These changes will be examined in detail in the next section.

III. SAMPLE STUDY

A. COMPUTATION OF OPTIMAL CPPMSMIR DIMENSIONS

To maximize the average torque, the objective function is considered according to eq. (24), the constraints of which are also given. Other dimensions of the machine that are fixed and that are not optimization parameters are presented in Table 1.

Three types of radial, parallel, and Halbach magnetization patterns are considered for optimization. The diagrams of the inverse changes of the average torque in terms of the number of repetitions for the three magnetization patterns are shown in Figs. 4.a, 4.b, and 4.c, respectively. Comparing these figures shows two points. First, all four algorithms converge to one point, ensuring the algorithms' correct operation. Second, the maximum torque is obtained for the Halbach magnetization pattern. Therefore, it is selected to optimize objective function. Also, PSO converges to the best solution faster, while GA needs more repetitions to reach the minimum. The specifications of the optimized CPPMSMIR are presented in Table 2.

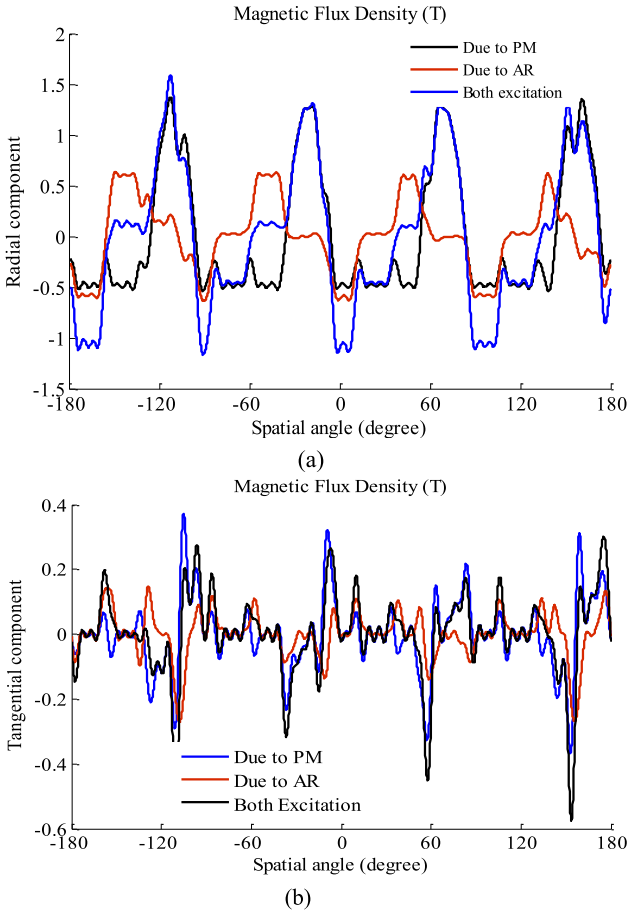

FIGURE 5. Magnetic flux density due to PM, AR and both a) radial component b) tangential component.

B. CALCULATION OF INDICATORS

Suppose the machine with the dimensions obtained is modeled by the two-dimensional method. In that case, the diagrams of the radial and tangential components of the magnetic flux density in the air gap in exchange for the excitation of the PM, the stator winding, and both are according to Figs. 5.a and 5.b. In accordance with these figures, the amplitude of the magnetic flux density which is created by PM is bigger than AR.

After calculating the magnetic flux density, according to Equations (6) to (9), all the components of torque, i.e., cogging torque, reluctance torque, and instantaneous torque, are calculated, the diagrams of which are shown in Figs. 6.a to 6.c. As can be seen from these figures, the

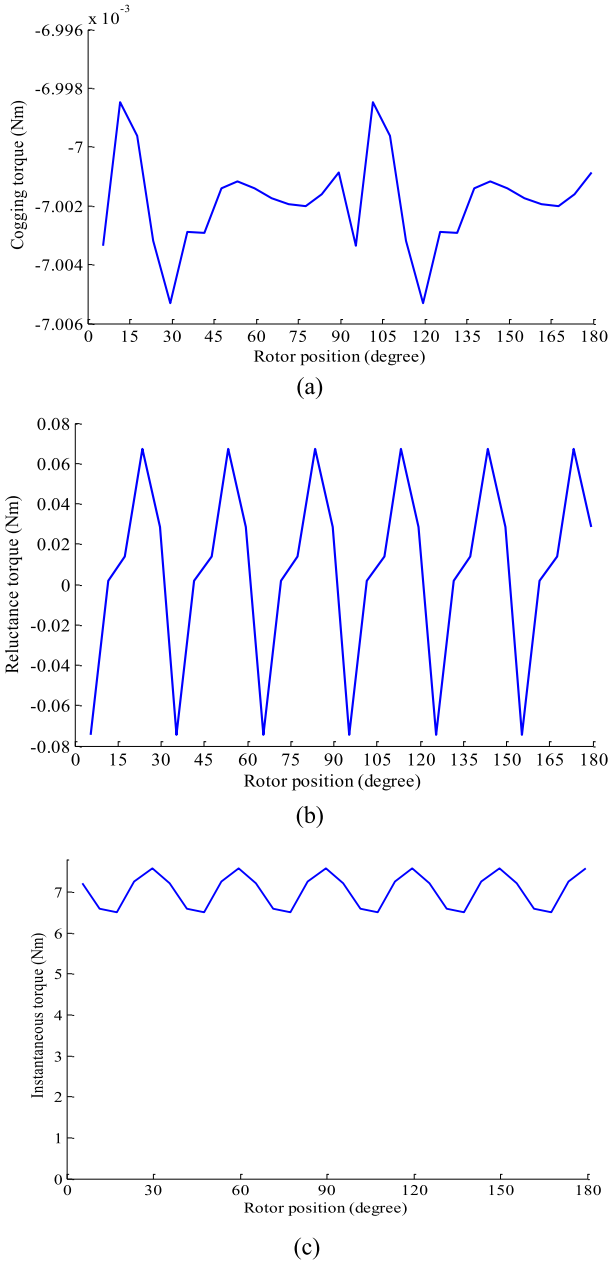

FIGURE 6. All components of torque a) cogging torque b) reluctance torque c) instantaneous torque.

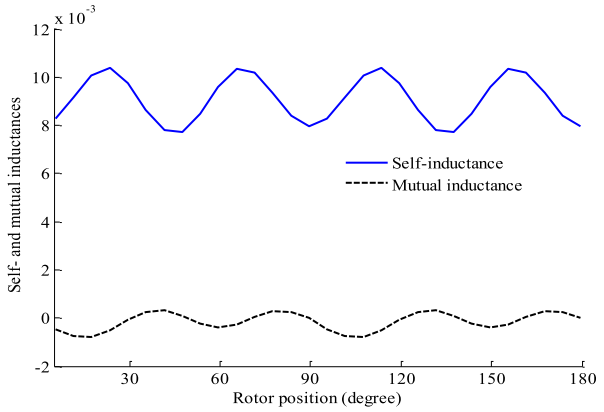

FIGURE 7. Self- and mutual inductance of stator winding.

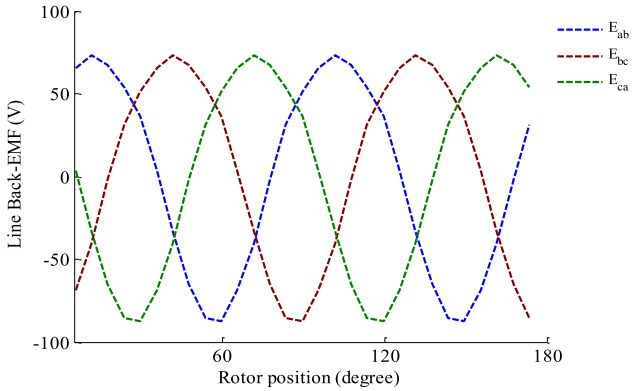

FIGURE 8. The Back-EMF for the consequent-pole machine.

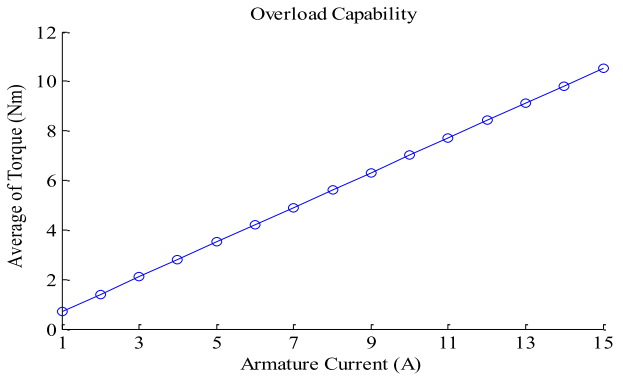

FIGURE 9. Overload capability.

cogging torque amplitude is very low and negligible, because the structure of the consequent pole has less PM than the superficial magnet and has less effect on the stator teeth.

Because the flux overlap of the windings of each phase is higher than that of the other phases, it is expected that the self-inductance of each phase will be higher than the mutual inductance between the two phases. Added to that, because the phase difference between the windings of one phase and the winding of the other phase is 60 and 120 degrees, and the flux of one phase affects the windings of the other phase with the cosine of the angle between them, the mutual inductance can have both positive and negative values. If the self- and mutual inductances of the stator windings are calculated using Equations (22) and (23) both said facts can be clearly seen in Fig. 7.

One of the most essential features of a synchronous machine is the induction voltage without harmonics because harmonics not only degrade the quality of power [21] but also increase losses [22]. The diagram of Back-EMF changes according to the rotor angle, as shown in Fig. 8. Not only is this figure within the permissible range of the IEEE-519 standard, but the three-phase symmetry is well established.

During the synchronous machine's operation, unforeseen overloads may occur due to sudden load changes or outages

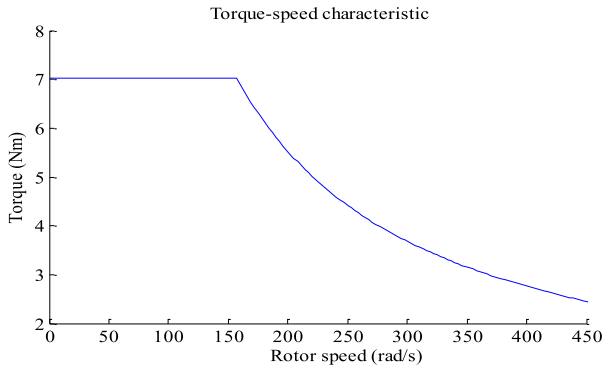

FIGURE 10. Torque-Speed characteristic for the optimal consequent-pole machine.

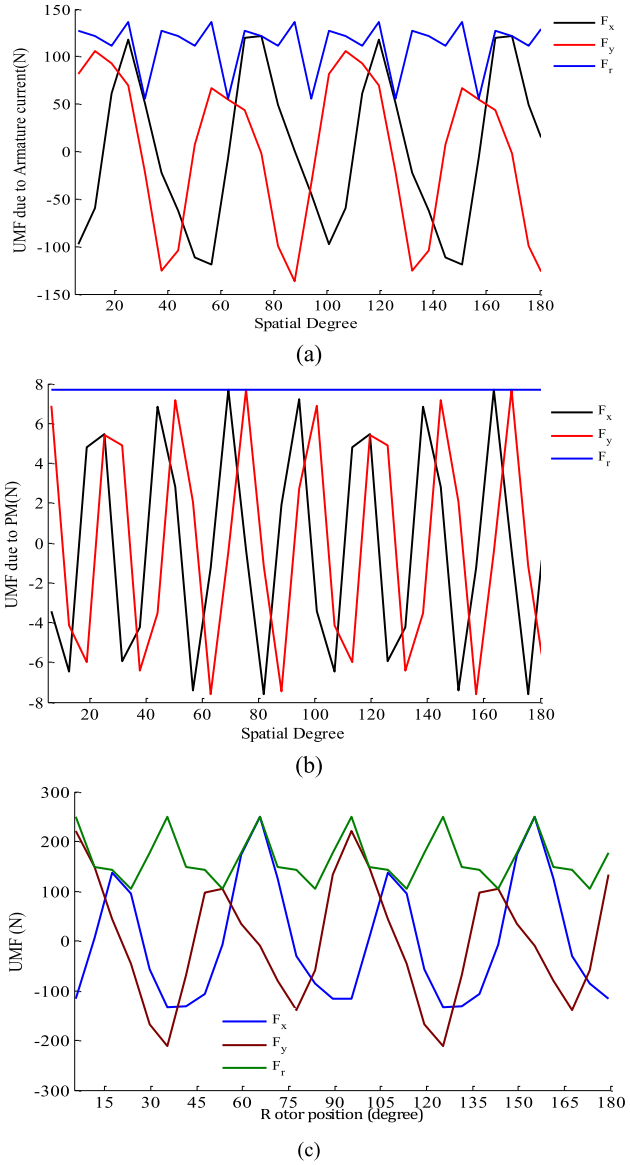

FIGURE 11. The magnitude of the UMF and its component in the X and Y directions due to a) armature current b) PM c) both excitations.

of other generators. The overload capability curve, shown in Fig. 9 for the optimized machine, examines the machine's

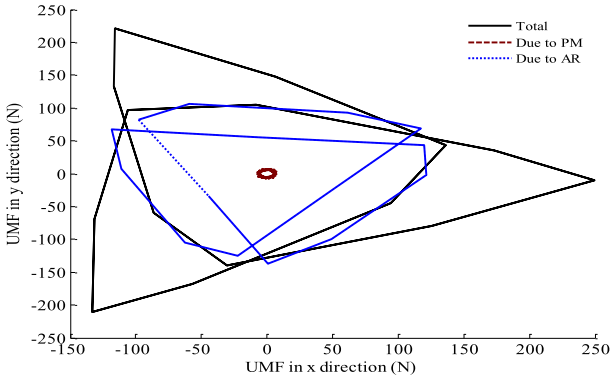

FIGURE 12. The UMF in the Y direction based on the UMF based on the X direction.

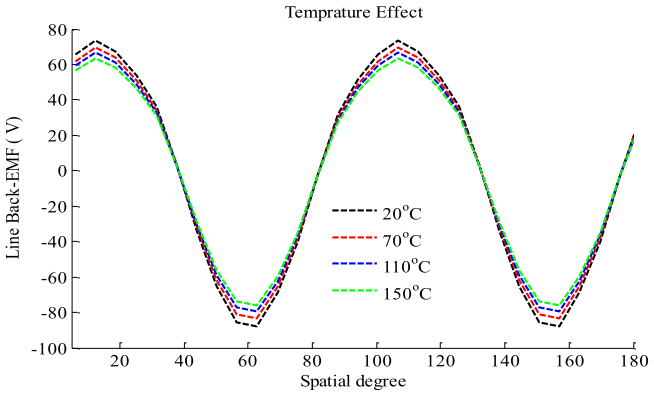

FIGURE 13. The Back-EMF due to the changes of temperature.

response to these problems. Given that the magnetic flux density due to the armature current is of less amplitude than the flux density resulting from PM, increasing it does not lead to saturation of the core; therefore, this diagram is linear.

In addition to CPPMSMIR performance at powers above the rated power, its performance at speeds above synchronous speed is another practical issue in machine design. The torque-speed diagram of the CPPMSMIR optimized up to 3 times the synchronous speed is shown in Fig 10. To reduce the output torque without changing the dimensions and excitation sources of the CPPMSMIR, the angle of the stator current must be adjusted accordingly.

UMFs are another factor that can limit the use of the machine, so the need to study them is inevitable. The magnitude of such forces and their values on the X and Y axes are important. Stator and PM excitation sources produce UMFs. The magnitude diagram of the UMFs and the diagram of their components in the direction of the X and Y axes per armature winding, PM, and both sources are shown in Figs. 11a, 11b, and 11c, respectively. Given the radial and tangential components of the Halbach magnetization pattern, it is expected that this pattern produces a fixed UMF amplitude. This fact is seen in Fig. 11b. Also, the UMF components in the said two directions relative to each other are plotted in Fig. 12. If the machine excitation sources are symmetrical, the amount of UMF is reduced to an acceptable level. According to Fig. 12,

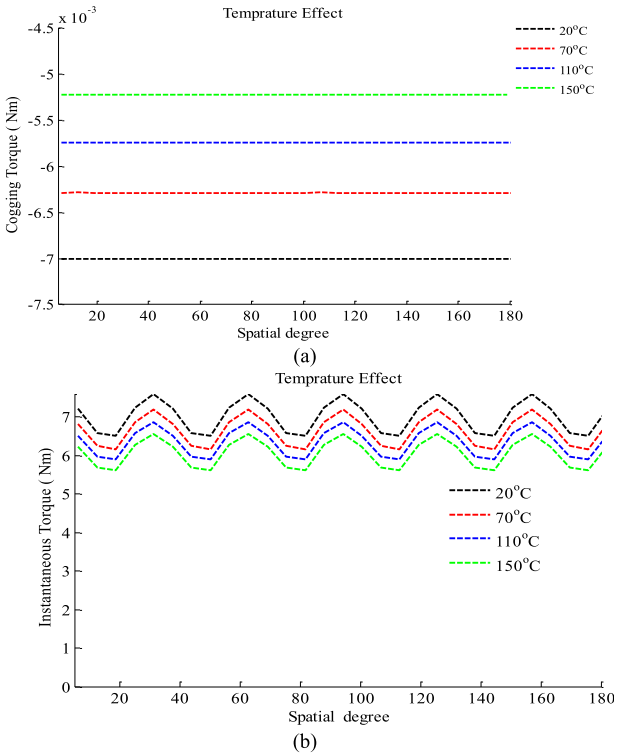

FIGURE 14. Changes of torque due to temperature a) cogging torque b) instantaneous torque.

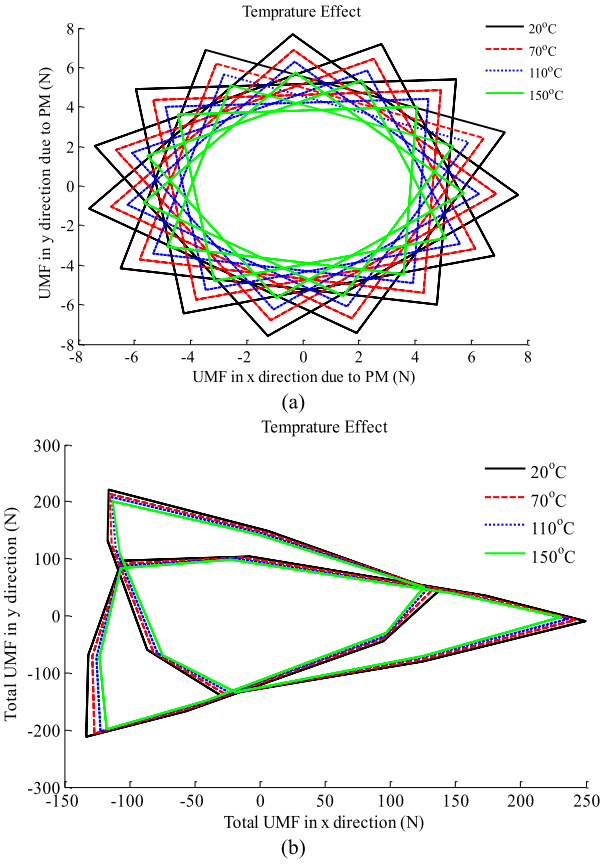

FIGURE 15. The UMF in the Y direction in terms of the UMF in the Y direction a) PM b) both excitation.

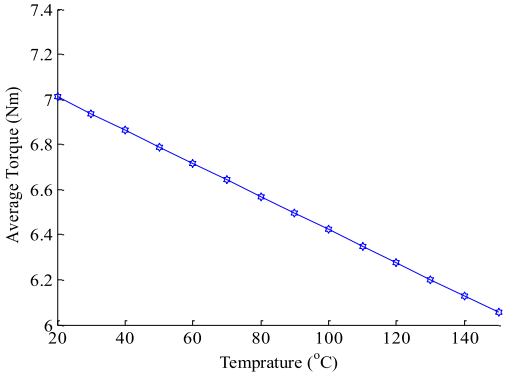

FIGURE 16. The average torque in terms of increasing temperature.

the PM excitation source has good symmetry, so its UMF level is acceptable; however, the armature coil has no diametric symmetry, so its UMF amplitude is greater than that of the PM. Also, the diagram resulting from both excitations in the figure shows that every 120 degrees of the diagram is drawn to one side. This fact indicates that for every 120 degrees, which is the axis of one phase, the effect of this phase is greater than the other two phases; between these points, all three phases affect the formation of UMF.

C. TEMPERATURE EFFECTS

As previously shown, increasing the temperature leads to a decrease in the residual flux density of the PM; hence, all indicators calculated according to it are affected. Self- and mutual inductances are constant because this parameter does not affect their calculation. Reducing the residual flux density of the magnet reduces the Back-EMF amplitude. This fact is shown in Fig. 13. In addition to the voltage, the magnitudes of the cogging and instantaneous torque decrease with reducing the residual magnetic flux density; this is while the reluctance torque remains constant because it results from the armature flux density. The diagrams of changes in these torques under the influence of temperature changes are shown in Figs 14.a and 14.b, respectively, which confirm the above point.

The UMFs, due to the armature reaction, do not change. The changes in $\boldsymbol{F_Y}$ in terms of $\boldsymbol{F_X}$. Fig. 15 plots the components for both cases. Attenuating the PM's residual flux density will certainly reduce the UMF resulting from the PM and the sum of the two excitation sources.

However, because the effect of the armature winding is greater than that of the PM due to the diagonal asymmetry on the total UMF, the total UMF does not change significantly. As previously shown, instantaneous torque decreases with an increase in temperature, so the average torque will behave similarly. The diagrams of average torque changes in temperature are shown in Fig. 16. The torque-speed characteristic and overload curves concerning temperature increase are also shown in Figs 17 and 18, respectively. It is seen in these

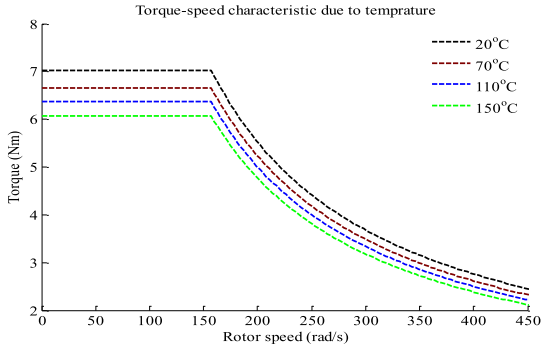

FIGURE 17. The torque-speed characteristics in terms of increasing temperature.

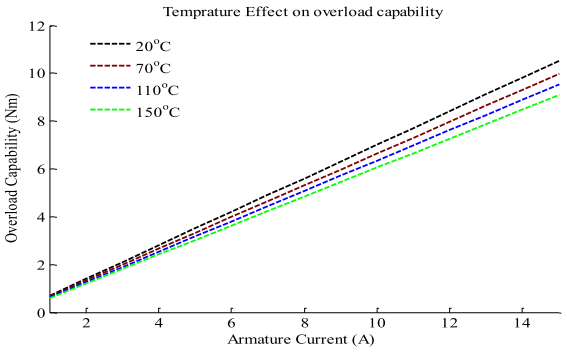

FIGURE 18. The overload capability in terms of increasing temperature.

figures that increase in the temperature leads to a decrease in torque, which is due to the attenuation of the residual magnetic flux density.

IV. CONCLUSION

This paper introduced a consequent-pole permanent magnet synchronous machine for use in electric vehicles. The consequent-pole machine has less costs, less loss, and more torque than a superficial magnet. Such machines are of two types, i.e., inner-rotor and outer-rotor consequent-pole machines. The outer-rotor consequent-pole machine has more torque, but the inner-rotor one has better heat removal and start-stop capability. Therefore, an inner-rotor machine is selected, and the torque-to-volume ratio needs to be maximized. First, the CPPMSMIR is modeled based on a two-dimensional method that is more efficient than equivalent and numerical circuit methods. Then, the torque per volume index is optimized with the four algorithms GA, PSO, DE and TLBO and three types of magnetization patterns. The convergence of all algorithms to one point indicates the correctness of their operation. The best solution is obtained for the bar magnet in shifting magnetization pattern. Then, all the components of torque, back-EMF, inductance, UMF on the X-axis, Y-axis, and their magnitudes resulting from the magnet, the armature reaction, and both excitation sources are calculated. The production of instantaneous torque with low ripple and sinusoidal back-EMF with low harmonic confirms the proper design of the machine. UMF due to PM/armature winding is low/high because of symmetry/asymmetry in this source.

The linear overload diagram shows the unsaturation of the machine. Also, by properly adjusting the armature current angle, the torque-speed characteristic can be extended up to several times the rated speed in the constant power region. Then, the effect of temperature on the residual flux density of the magnet is investigated. Reduction of residual flux density, albeit not affecting reluctance torque, inductance and UMF resulting from armature flux, reduces the magnitudes of cogging torque, instantaneous torque, average torque, Back-EMF range, and UMFs due to the PM and both excitation sources. However, the changes that occur in the whole UMF are slight and negligible because in this CPPMSMIR, the UMF is more affected by the armature current than the PM. In addition, an increase in the temperature also affects the overload capability and torque-speed characteristic of the CPPMSMIR at less and more than the rated speed.

The proposed model can be utilized for optimization of a large number of objective functions such as decreasing torque ripple. Besides, it validates multi-objective optimization and other design targets.

REFERENCES

[1] J. R. Hendershot and T. J. E. Miller, *Design of Brushless Permanent Magnet Motors*. London, U.K.: Oxford Univ. Press, 1994.
[2] D. G. Dorrell, M.-F. Hsieh, and Y. Guo, "Unbalanced magnet pull in large brushless rare-Earth permanent magnet motors with rotor eccentricity," *IEEE Trans. Magn.*, vol. 45, no. 10, pp. 4586–4589, Oct. 2009.
[3] S. Teymoori, A. Rahideh, H. Moayed-Jahromi, and M. Mardaneh, "Two-dimensional analytical magnetic field prediction for consequent-pole permanent magnet synchronous machines," *IEEE Trans. Magn.*, vol. 52, no. 6, pp. 4215–4218, Sep. 2016.
[4] S.-U. Chung, D.-H. Kang, J.-H. Chang, J.-W. Kim, and J.-Y. Lee, "New configuration of flux reversal linear synchronous motor," in *Proc. Int. Conf. Electr. Mach. Syst. (ICEMS)*, Oct. 2007, pp. 864–867.
[5] S.-U. Chung, J.-W. Kim, B.-C. Woo, D.-K. Hong, J.-Y. Lee, and D.-H. Koo, "A novel design of modular three-phase permanent magnet Vernier machine with consequent pole rotor," *IEEE Trans. Magn.*, vol. 47, no. 10, pp. 4215–4218, Oct. 2011.
[6] A. Hoseinpour, M. Mardaneh, and A. Rahideh, "Investigation of the effects of different magnetization patterns on the performance of series hybrid excitation synchronous machines," *Prog. Electromagn. Res. M*, vol. 64, pp. 109–121, 2018.
[7] A. Hosseinpour, M. Mardaneh, and A. Rahideh, "Two-dimensional analytical model for double field excitation synchronous machines," *IET Gener., Transmiss. Distribution*, vol. 15, no. 6, pp. 1081–1093, Mar. 2021.
[8] A. Ghaffari, A. Rahideh, H. Moayed-Jahromi, A. Vahaj, A. Mahmoudi, and W. L. Soong, "2-D analytical model for outer-rotor consequent-pole brushless PM machines," *IEEE Trans. Energy Convers.*, vol. 34, no. 4, pp. 2226–2234, Dec. 2019.
[9] A. Hosseinpour and A. Khajeh, "Determine optimal value of pole arc to pole pitch ratio in order to increasing average torque and decreasing unbalance magnetic force in hybrid electrical vehicle," *Int. J. Ind. Electron., Control Optim.*, vol. 4, no. 4, pp. 445–451, 2021.
[10] A. Hoseynpour and M. Oukatisadeq, "Optimal design of electric machine used in spacecraft by using fuzzy multi-objective particle swarm algorithm," *Fuzzy Syst. Appl.*, vol. 4, no. 2, pp. 151–164, 2022.
[11] H. Dhulipati, S. Mukundan, Z. Li, E. Ghosh, J. Tjong, and N. C. Kar, "Torque performance enhancement in consequent pole PMSM based on magnet pole shape optimization for direct-drive EV," *IEEE Trans. Magn.*, vol. 57, no. 2, pp. 1–7, Feb. 2021.
[12] G. Xu, W. Zhao, G. Liu, F. Zhai, and Q. Chen, "Torque performance improvement of consequent-pole PM motors with hybrid rotor configuration," *IEEE Trans. Transport. Electrific.*, vol. 7, no. 3, pp. 1561–1572, Sep. 2021.

[13] Q. Chen, G. Liu, W. Zhao, and M. Shao, "Nonlinear adaptive lumped parameter magnetic circuit analysis for spoke-type fault-tolerant permanent-magnet motors," *IEEE Trans. Magn.*, vol. 49, no. 9, pp. 5150–5157, Sep. 2013.
[14] A. Hosseinpour and M. O. Sadeq, "Harmonic reduction of current by using phase shifting and shunt-active filter trained by fuzzy particle swarm optimization," *Int. J. Fuzzy Syst.*, vol. 24, no. 6, pp. 2729–2739, Sep. 2022.
[15] J. Jiang, Q. Jiang, and S. Xiao, "Electromagnetic optimization of single-sided linear induction motors based on the genetic algorithm," in *Proc. Int. Conf. Intell. Comput., Autom. Syst.*, Dec. 2019, pp. 329–334.
[16] D. Fodorean, L. Idoumghar, M. Brévilliers, P. Minciunescu, and C. Irimia, "Hybrid differential evolution algorithm employed for the optimum design of a high-speed PMSM used for EV propulsion," *IEEE Trans. Ind. Electron.*, vol. 64, no. 12, pp. 9824–9833, Dec. 2017.
[17] R. V. Rao, V. J. Savsani, and D. P. Vakharia, "Teaching-learning-based optimization: A novel method for constrained mechanical design optimization problems," *Comput.-Aided Des.*, vol. 43, no. 3, pp. 303–315, 2011.
[18] A. Abbas and A. Iqbal, "A subdomain model for armature reaction field and open-circuit field prediction in consequent pole permanent magnet machines," *Int. J. Numer. Modelling, Electron. Netw., Devices Fields*, vol. 35, no. 6, p. e3023, Nov. 2022.
[19] A. Abbas, A. Iqbal, A. Hosseinpour, M. Shahabuddin, and E. Kabalci, "Investigation of the effect of the temperature and magnetization pattern on flux density, instantaneous torque, unbalanced magnetic forces of a surface inset PMM," in *Proc. 4th Global Power, Energy Commun. Conf. (GPECOM)*, Jun. 2022, pp. 190–195.
[20] J. F. Geras and M. Wing, *Permanent Magnet Motor Topology Design and Application*. New York, NY, USA: Marcel Dekker Inc, 2002.
[21] A. Hoseinpour, "Three phase active filter with four switching inverter and variable index modulation," in *Proc. 1st Power Qual. Conf.*, Sep. 2010, pp. 1–7.
[22] A. Hoseinpour and R. Ghazi, "Harmonic reduction in wind turbine generators using a shunt active filter," *Int. Rev. Model. Simulations*, vol. 5, no. 2, pp. 722–730, Apr. 2012.

ALIREZA HOSSEINPOUR was born in Zabol, Iran, in 1985. He received the B.Sc. degree (Hons.) in electrical engineering from the University of Sistan and Baluchestan, Zahedan, Iran, in 2007, the M.Sc. degree in electrical engineering from the Ferdowsi University of Mashhad, Iran, in 2010, and the Ph.D. degree in electrical engineering from the Shiraz University of Technology, in 2018. Following receipt of the Ph.D. degree, he joined the University of Zabol, Zabol. His research interests include wind turbines, renewable energy, permanent magnet synchronous machine drives, four-switch three-phase inverters, power electronics, and the design of hybrid electrical vehicles.

AHMED ABBAS received the B.Sc. degree in electrical engineering from Kordofan University, Sudan, in 2014, and the M.Tech. degree in power electronics and drives from the National Institute of Technology (NIT), Warangal, India, in 2017. Currently he is a Research Assistant with the Department of Electrical Engineering, Gdansk University of Technology, Gdansk, Poland. His research interests include multi-level inverter, open-end winding induction motor drives, multiphase machines, and analytical models of electrical machines.

MAHMOUD OUKATI SADEGH was born in Zabol, Iran, in 1966. He received the B.Sc. and M.Sc. degrees in electrical power system engineering from Tehran University, Tehran, Iran, in 1989 and 1992, respectively, and the Ph.D. degree in electrical engineering from Strathclyde University, Glasgow, U.K., in 2003. Currently, he is an Associate Professor with the Department of Electrical and Engineering, University of Sistan and Baluchestan, Zahedan, Iran. His research interests include power system control and operation, electrical distribution systems, power electronics, and smart grid.

ATIF IQBAL (Fellow, IEEE) received the B.Sc. (Hons.) and M.Sc.Eng. degrees in power systems and drives from Aligarh Muslim University (AMU), Aligarh, India, in 1991 and 1996, respectively, the Ph.D. degree from Liverpool John Moores University, Liverpool, U.K., in 2006, and the D.Sc. (Habilitation) degree in control, informatics, and electrical engineering from Gdańsk University of Technology, Poland, in 2019. He has been a Lecturer with the Department of Electrical Engineering, AMU, since 1991, where he was a Full Professor, until August 2016. He is currently a Full Professor with the Department of Electrical Engineering, Qatar University, Doha, Qatar, and a former Full Professor with the Department of Electrical Engineering, AMU. He has published widely in international journals and conferences his research findings related to power electronics, variable speed drives, and renewable energy sources. He has authored/coauthored more than 450 research articles and four books and several chapters in edited books. He has supervised several large research and development projects worth more than multi-million USD. He has supervised and co-supervised several Ph.D. students. His research interests include smart grids, complex energy transition, active distribution networks, electric vehicles drivetrain, sustainable development and energy security, distributed energy generation, and multiphase motor drive systems. He is a fellow of IET, U.K., and IE, India. He was a recipient of the Outstanding Faculty Merit Award, from 2014 to 2015, and the Research Excellence Awards from Qatar University, in 2015 and 2019. He was a recipient of the Maulana Tufail Ahmad Gold Medal from AMU, in 1991, for standing first at the B.Sc.Eng. (electrical) exams. He has received several best research papers awards, such as IEEE ICIT-2013, IET-SEISCON-2013, SIGMA 2018, IEEE CENCON 2019, IEEE ICIOT 2020, ICSTEESD-20, and Springer ICRP 2020. He was the Vice-Chair of the IEEE Qatar Section. He is an Associate Editor of IEEE TRANSACTIONS ON INDUSTRIAL ELECTRONICS and IEEE ACCESS, the Editor-in-Chief of the *Journal of Electrical Engineering* (I'Manager), a former Associate Editor of IEEE TRANSACTION ON INDUSTRY APPLICATION, and a former Guest Associate Editor of IEEE TRANSACTIONS ON POWER ELECTRONICS.

AYMEN FLAH was born in Gabès, Tunisia, in 1983. He received the bachelor's degree in electrical engineering and the M.Tech. degree from ENIG, Tunisia, in 2007 and 2009, respectively, and the Ph.D. degree from the Department of Electrical Engineering, in 2012. He has academic experience of 11 years. He has published more than 100 research articles in reputed journals and more than 40 research papers in international conferences and book chapters. His research interests include electric vehicles, power systems, and renewable energy.

LUKAS PROKOP received the Ing. degree in electrical power engineering from the Faculty of Electrical Engineering and Communication, Brno University of Technology. He is currently an Associate Professor with the Faculty of Electrical Engineering and Computer Science, VSB—Technical University of Ostrava. He is also engaged in renewable energy sources, modern technologies, and methods in electrical power engineering and electrical measurements. He is currently a Research Team Member of Czech and international research projects. He is also the Deputy Head of the ENET Research Centre.

ENAS ALI received the Ph.D. degree, in 2021. She is currently an Adjunct Assistant Professor with University Centre for Research and Development, Chandigarh University, Punjab, India. Her research interest includes AI techniques in engineering applications.

RAMY N. R. GHALY (Student Member, IEEE) received the B.Sc. degree from the Faculty of Industrial Education, Ministry of Higher Education, Cairo, in 2001, and the M.Sc. and Ph.D. degrees from the Faculty of Industrial Education, Suez University, Suez, in 2013 to 2019, respectively. He was an Electric Power Instructor (part-time) with the Faculty of Industrial Education, Ministry of Higher Education, from 2001 to 2003. He has been an Electric Power Instructor (full-time) with the Mataria Industrial Technical Institute, Ministry of Higher Education, since 2003. He participated in teaching with the Electrical and Electronic Department with faculty members at the Northampton Community College, Pennsylvania, USA, from 2008 to 2009, via the Fulbright Program. He has been an ILVP Member with the Department of State, USA, since 2015. His research interests include high-voltage areas, especially grounding systems and power transformers.